Article

Not peer-reviewed version

Enhanced Luminescence and Thermal Stability in High Gd^{3+}/Eu^{3+} Co-Doped $Ba_3Y_4O_9$ Phosphors via Co-Precipitation Method

Dong Zhu , Chunfeng Wang , Xiaohuai Wang * , Shun Han , Peijiang Cao , Yuxiang Zeng , Ming Fang , Wenjun Liu , Deliang Zhu , Youming Lu *

Posted Date: 3 February 2025

doi: 10.20944/preprints202502.0012.v1

Keywords: Gd^{3+} doping; thermal stability; luminescence enhancement; energy transfer

Article

Enhanced Luminescence and Thermal Stability in High Gd^{3+}/Eu^{3+} Co-Doped $Ba_3Y_4O_9$ Phosphors via Co-Precipitation Method

Dong Zhu [1,2], Chunfeng Wang [1], Xiaohuai Wang [3,*], Shun Han [1], Peijiang Cao [1], Yuxiang Zeng [1], Ming Fang [1], Wenjun Liu [1], Deliang Zhu [1] and Youming Lu [1,3,*]

[1] College of Materials Science and Engineering, Guangdong Research Center for Interfacial Engineering of Functional Materials, Shenzhen University, Shenzhen, 518060 PR China.

[2] College of Physics and Optoelectronic Engineering, Shenzhen University, Shenzhen, 518060 PR China.

[3] Department of Physics and Electronic Engineering, Hanshan Normal University, Chaozhou, 521041 PR China.

* Correspondence: wxh1997@hstc.edu.cn (X.W.) and ymlu@szu.edu.cn (Y.L.)

Abstract: The co-precipitation method was successfully used to synthesize BYGO: Eu^{3+} phosphors with high Gd^{3+} doping, resulting in significantly enhanced thermal stability and luminescence performance. Structural analyses confirm that Gd^{3+} and Eu^{3+} ions substitute Y^{3+} in the lattice, causing lattice expansion and improving crystal asymmetry, which enhances Eu^{3+} emission. The incorporation of Gd^{3+} creates efficient energy transfer pathways to Eu^{3+} while suppressing non-radiative relaxation, leading to stable fluorescence lifetimes even at elevated temperatures. With a thermal activation energy of ~0.3051 eV, the BYGO: Eu^{3+} system exhibits superior resistance to thermal quenching compared to BYO: Eu^{3+} and many conventional red phosphors. Furthermore, the reduced color temperature and stable emission spectra across a wide temperature range highlight its potential for advanced lighting and display technologies in high-temperature environments.

Keywords: Gd^{3+} doping; thermal stability; luminescence enhancement; energy transfer

1. Introduction

Inorganic phosphors play a crucial role in white light-emitting diodes (W-LEDs) due to their high luminous efficiency, strong brightness, and long operational lifespan, making them indispensable in the lighting industry. The most advanced commercial W-LEDs typically combine gallium nitride (GaN) blue LED chips with $Y_3Al_5O_{12}$: Ce^{3+} yellow phosphors [1–3]. However, these systems face limitations, including a low color rendering index and high correlated color temperature (CCT), primarily due to insufficient red emission from the phosphor and the dominance of blue light emitted by the LED chip [4,5]. Moreover, the performance of red phosphors often deteriorates under high-temperature conditions, as their emission intensity is affected by radiation transitions and the thermal effects of the chip, further limiting their practical applications in scenarios requiring vivid color rendering. To overcome these challenges, recent research has focused on UV-excited phosphors, utilizing red, green, and blue tricolor emissions to generate white light [6–8]. By optimizing doping levels and selecting appropriate tricolor phosphor combinations, W-LEDs with low CCT, high brightness, and superior color quality can be achieved [9–12]. Enhancing the red emission intensity and thermal stability of phosphors remains a critical objective for advancing next-generation W-LED technologies suitable for high-performance lighting applications.

Phosphor materials for W-LEDs generally feature an inert host lattice that provides a stable luminescent environment, with optically active ions serving as activators. $Ba_3Y_4O_9$ (BYO) has emerged as a promising host material for red phosphors due to its unique physicochemical properties [13–16]. Compared to conventional hosts like Y_2O_3 and Gd_2O_3, BYO offers superior structural

 doi:10.20944/preprints202502.0012.v1

stability, an optimal bandgap (~3.436 eV), lower phonon energy, and a higher proportion of asymmetric lattice sites, making it highly compatible with Eu^{3+} doping [17,18]. The *4f* energy levels of Eu^{3+} lie outside BYO's band structure and align well with its electronic configuration, facilitating the formation of discrete luminescent centers [19]. However, the luminescence efficiency of BYO: Eu^{3+} decreases significantly at elevated temperatures, limiting its practical application in high-temperature environments [20]. Enhancing the thermal stability and high-temperature performance of BYO: Eu^{3+} is therefore essential for advancing its utility in lighting technologies.

The absorption spectrum of Eu^{3+} primarily involves 4f-4f transitions. These transitions are parity-forbidden for electric dipole transitions and only allow weak magnetic dipole transitions, resulting in narrow bands and low absorption efficiency [21–23]. When the electrons in the *2p* orbitals of ligand oxygen (O^{2-}) are transferred to the partially filled *4f* orbitals of Eu^{3+}, a broad charge transfer band (CTB) appears in the excitation spectrum, significantly enhancing the absorption of excitation energy[24,25]. However, due to the limited intensity of *f-f* transitions in rare-earth ions, the direct excitation efficiency of Eu^{3+} is low. To address this, Gd^{3+} is introduced as a sensitizer, whose characteristic excitation peaks overlap with the CTB of Eu^{3+}, enabling efficient energy absorption and transfer, thereby enhancing the luminescence efficiency of Eu^{3+} [26]. With its half-filled f^7 configuration, Gd^{3+} exhibits $^8S_7/_2 \rightarrow {}^6I_j$ and $^8S_7/_2 \rightarrow {}^6P_j$ transitions that partially overlap with the CTB of Eu^{3+}, facilitating efficient energy transfer. Li et al. demonstrated that Eu^{3+} emission behavior in Y_2O_3 and $(Y_{0.75}Gd_{0.25})_2O_3$ revealed this overlap but lacked a mechanistic model for explanation [27]. Mancic et al. demonstrated that substituting Y^{3+} with Gd^{3+} in $LnTeBO_5$ stabilized the lattice, reduced the charge transfer barrier, and improved luminescence intensity and thermal stability, though the thermal activation energy remained low at ~0.26 eV [28]. In this study, BYGO:Eu^{3+} precursor materials were synthesized via a co-precipitation method, and rapid high-temperature annealing successfully stabilized a high Gd^{3+} doping concentration of 40 a.t.% within the BYO lattice, far exceeding the reported limit of 12% [29]. By analyzing the characteristic emission peaks of Gd^{3+} and Eu^{3+}, an energy transfer model from $Gd^{3+} \rightarrow Eu^{3+}$ was established. Thermal quenching experiments demonstrated excellent thermal stability, while the consistent CCT values at elevated temperatures further confirmed that BYGO: Eu^{3+} phosphors are promising candidates for W-LED applications in high-temperature environments.

2. Results and Discussion

Figure 1a illustrates the synthesis process of BYGO: Eu^{3+} phosphors using a co-precipitation method. First, precursor solutions were prepared in specific proportions and fully dissolved. These solutions were then slowly added dropwise into an ammonium bicarbonate solution using a separatory funnel. Throughout the titration process, the solution's pH was continuously monitored with a pH meter and maintained at 10 by adding ammonium hydroxide. After titration, the mixture was stirred for an additional 6 hours to ensure a complete reaction. The resulting precipitate was washed multiple times, with the final wash performed using n-hexane to remove any residual organic impurities. The washed product was dried at 60 °C for 12 hours in an oven to obtain the precursor. This precursor was then calcined at a ramping rate of 1 °C /min to 1400 °C, held at the target temperature for 6 hours, and rapidly cooled to room temperature to yield the BYGO: Eu^{3+} phosphors. **Figure 1b** shows the SEM images of the BYGO: Eu^{3+} phosphors synthesized by the co-precipitation method. The phosphor particles are approximately 1 μm in size, exhibiting irregular shapes and noticeable voids between particles. These voids are attributed to the decomposition of HCO_3^- and CO_3^{2-} in the precursor during heating [30]. The connections between particles result from the sintering process, where ~40 nm precursor particles underwent grain growth during high-temperature calcination (**Figure S1**). Energy-dispersive spectroscopy (EDS) mapping confirms the uniform distribution of Ba, Y, Gd, Eu, and O elements throughout the phosphors, which facilitates more efficient luminescence performance.

Figure 1c presents high-resolution transmission electron microscopy (HR-TEM) images of BYGO: Eu^{3+} phosphors. The particles exhibit slight aggregation, and their size aligns with the SEM

 doi:10.20944/preprints202502.0012.v1

results. The selected area electron diffraction (SAED) pattern reveals bright spot rings, indicating high crystallinity and confirming the formation of a polycrystalline BYO host structure consistent with JCPDS *No.038-1377*. In the HRTEM images of the optimized nanoscale samples, distinctive lattice fringes are observed with an interplanar spacing of 3.094 Å, closely matching the standard value of 2.7954 Å for the (1 0 7) crystal plane of the $Ba_3Y_4O_9$ host. However, the spacing is increased by ~0.1186 Å, indicating a lattice expansion of approximately 4.0%. This expansion results from the substitution of Y^{3+} ions with larger Gd^{3+} and Eu^{3+} ions in the BYO lattice. **Figure 1d** displays the XRD patterns of undoped and doped BYO samples. All patterns match well with the standard $Ba_3Y_4O_9$ data, with no additional diffraction peaks observed, confirming that the dopant ions were fully incorporated into the BYO lattice without forming impurity phases. The magnified main peak detail on the right further reveals that, with the doping of Eu^{3+} and Gd^{3+}, all diffraction peaks shift toward smaller angles, accompanied by a deterioration in crystallinity. This indicates that the excessive substitution of the original lattice Y^{3+} ions by the larger Gd^{3+} and Eu^{3+} ions leads to lattice expansion and structural changes.

Figure 2a presents the PLE spectra of Eu^{3+}-doped BYO and BYGO systems, showing two primary components. The first component is a broadband excitation peak centered at 258 nm (CTB), spanning the 220–330 nm short-wavelength region. This peak arises from the charge transfer transition of electrons from the *2p* orbitals of O^{2-} to the empty *4f* orbitals of Eu^{3+}, forming an excited state [24]. The second component consists of several sharp excitation peaks in the 313–538 nm long-wavelength region, corresponding to the *4f-4f* transitions of Eu^{3+}. These include ~363 nm ($^7F_0 \rightarrow {}^5D_4$), ~385 nm ($^7F_0 \rightarrow {}^5G_4$), ~395 nm ($^7F_0 \rightarrow {}^5L_6$), ~417 nm ($^7F_0 \rightarrow {}^5D_3$), ~465 nm ($^7F_0 \rightarrow {}^5D_2$), and ~538 nm ($^7F_0 \rightarrow {}^5D_1$) [31]. Among these, the CTB intensity is significantly higher than that of the intra-4*f* transitions, indicating that CTB excitation is the most effective method to achieve fluorescence in the Eu^{3+}-doped BYO system. Notably, the peak at 394 nm ($^7F_0 \rightarrow {}^5L_6$) exhibits the highest intensity among the *4f-4f* transitions [32]. This hypersensitive transition is highly dependent on the strength of the crystal field, meaning even minor variations in the local structure or surrounding environment of Eu^{3+} can significantly affect its intensity. Additionally, two extra peaks at 275 nm and 315 nm appear in the BYGO system, attributed to the $^8S_{7/2} \rightarrow {}^6I_J$ and $^8S_{7/2} \rightarrow {}^6P_J$ transitions of Gd^{3+}. The 275 nm peak overlaps with the CTB, enabling efficient energy transfer from $Gd^{3+} \rightarrow Eu^{3+}$ [33]. **Figure 2b** shows the PL spectra of Eu^{3+}-doped BYO and BYGO systems under 258 nm (CTB) excitation. Six emission peaks are detected, with the most prominent one at ~612 nm ($^5D_0 \rightarrow {}^7F_2$), which corresponds to an electric dipole transition [34]. This transition is highly sensitive to lattice asymmetry due to the symmetry-breaking effect of the *4f* orbitals in non-centrosymmetric environments. The split peaks in the orange region (~589 nm, ~595 nm, and ~601 nm) result from the magnetic dipole transition ($^5D_0 \rightarrow {}^7F_1$), which occurs in centrosymmetric environments. The asymmetry of the Eu^{3+} local environment is reflected in the intensity ratio (IR/O) of the $^5D_0 \rightarrow {}^7F_2$ and $^5D_0 \rightarrow {}^7F_1$ transitions. In the BYO system, the IR/O value is 2.92, indicating a highly asymmetric local environment for Eu^{3+} ions. In the BYGO system, the IR/O ratio increases slightly (~3.06), attributed to the lattice expansion caused by the larger ionic radius of Gd^{3+} (~1.053 Å, CN=8) compared to Y^{3+} (~1.040 Å, CN=8), which enhances asymmetry. Additionally, as a common sensitizer, Gd^{3+} significantly enhances Eu^{3+} emission, increasing the overall PL intensity of BYGO by ~135% compared to BYO under identical conditions (**Figure S2**). The inset shows the emission intensity trend for different Eu^{3+} doping concentrations, consistent with previously reported studies [35].

Figure 2c evaluates the quantum efficiency (QE), a critical parameter determining phosphor brightness (see **Note S1** for QE calculation). For BYO and BYGO systems, the maximum QE is achieved at the quenching concentration (~5% Eu^{3+}), reaching ~55% and ~86%, respectively (**Figure S3**). The QE trends align with those of the PL intensity, confirming that doping concentration strongly influences luminescence properties. In the Gd^{3+}/Eu^{3+} co-doped systems, Martins et al. measured a quantum efficiency (QE) of 48% in Y_2O_3 [36], while Liu et al. reported a QE of 70.6% in $LiGd_{0.5}Eu_{0.5}MgWO_6$ [37], both of which are lower than that of BYGO system.

 doi:10.20944/preprints202502.0012.v1

To confirm the substitution of Y^{3+} by Gd^{3+} in the BYO lattice, **Figure 2d-f** presents the Rietveld refinement results for BYO, BYO: 5% Eu^{3+}, and BYGO: 5% Eu^{3+}, analyzed using Topas software. Comparative analyses of the structural parameters are summarized in **Table S1**, with refinement parameters detailed in **Tables S2–S4**. The results confirm that the ionic radii of Gd^{3+} (~0.938 Å, CN=6; ~1.053 Å, CN=8) and Eu^{3+} (~0.950 Å, CN=6; ~1.066 Å, CN=8) are larger than that of Y^{3+}, making excessive doping prone to introducing impurity phases. However, the use of chemical co-precipitation and rapid cooling at 1350 °C effectively traps impurity ions within the lattice, reducing their escape probability. Calculations indicate that ~4.9 at.% Eu^{3+} and ~38.15 at.% Gd^{3+} successfully replaced Y^{3+} sites, with the lattice volume expanding by ~3.19%. This conclusion is consistent with the lattice expansion observed in the TEM results (**Figure 1c**).

Excessive doping of Gd^{3+} not only influences the lattice sites but also modifies the original luminescence mechanism in the BYO: Eu^{3+} system [36]. To investigate the role of Gd^{3+} as a sensitizer in enhancing luminescence in the BYGO: Eu^{3+} system, PLE spectra were measured using the characteristic emission wavelength of Gd^{3+} at ~315 nm as the monitoring wavelength, as shown in **Figure 3a(i)**. The spectra reveal a distinct excitation peak at ~275 nm corresponding to the $^8S_{7/2} \rightarrow {}^6P_j$ transition, along with additional peaks at ~244 nm and ~252 nm, attributed to the $^8S_{7/2} \rightarrow {}^6I_j$ transitions. These peaks are absent in the PLE spectra of BYO: 5% Eu^{3+}, confirming that they are directly related to the presence of Gd^{3+}. **Figure 3a(ii)** demonstrates a positive correlation between peak intensity and Gd^{3+} concentration, but when the Gd^{3+} content exceeds 40%, a phase transition occurs in the BYGO system, as shown in **Figure S4**, establishing 40% as the maximum doping level to maintain the pure-phase structure. PL spectra under different monitoring wavelengths are presented in **Figure 3b**. For BYO: 5% Eu^{3+}, the PL intensity is weak when excitation wavelength at 275 nm, as this wavelength lies within the CTB excitation range of Eu^{3+}. In contrast, the PL spectrum of BYGO: 5% Eu^{3+} shows not only the characteristic emission peaks of Eu^{3+} but also a strong emission peak at ~315 nm corresponding to the $^6P_j \rightarrow {}^8S_{7/2}$ transition of Gd^{3+}. This indicates that a significant portion of the ultraviolet energy absorbed by the system is released as Gd^{3+} emission, while only a small fraction is transferred to Eu^{3+} through energy transfer, as shown in **Figure 3b(i)**. When the monitoring wavelength is shifted to 258 nm (**Figure 3b(ii)**), the Gd^{3+} emission peaks are nearly absent, leaving only the strong characteristic emissions of Eu^{3+}. This suggests that under 258 nm excitation, nearly all energy in the system is efficiently transferred to Eu^{3+}.

Based on the Judd-Ofelt theory, the energy transfer mechanism in the BYGO: Eu^{3+} system is depicted in **Figure 3c**. At an excitation wavelength of 275 nm, the BYO: Eu^{3+} system shows weak emission because, although this wavelength is not the optimal excitation wavelength, it still falls within the CTB region of Eu^{3+}, allowing for low-efficiency photon absorption. In contrast, the BYGO: Eu^{3+} system exhibits a sharp and intense ultraviolet emission (~315 nm). This energy corresponds to the transition of Gd^{3+} from the $^8S_{7/2} \rightarrow {}^6I_J$ energy level, with a portion of the energy transferred to Eu^{3+}, as the $6I_j$ level overlaps with Eu^{3+}'s CTB. Additionally, some Gd^{3+} ions undergo the $^6I_J \rightarrow {}^6P_J$ transition, and the energy difference generated in this process is suitable for Eu^{3+}'s $^5D_0$ energy level absorption, promoting the characteristic Eu^{3+} emission [38]. Therefore, as shown in **Figure 3b i**, the emission intensity of BYGO: Eu^{3+} at 612 nm is stronger than that of BYO: Eu^{3+}. At an excitation wavelength of 258 nm, the BYO: Eu^{3+} system directly absorbs photon energy, with electrons transitioning from the ground state $^7F_0$ to the CTB and subsequently relaxing non-radiatively to the $^5D_0$ excited state. This is followed by a radiative transition to the ^7F_J ($J = 0, 1, 2, 3, 4$) states, emitting orange-red light. In the BYGO: Eu^{3+} system, electrons transition from the $^8S_{7/2} \rightarrow {}^6D_J$, with energy transfer occurring through multiple Gd^{3+} ions in the lattice, concentrating the excitation energy onto a few high-energy Gd^{3+} ions. These high-energy Gd^{3+} ions then efficiently transfer energy to Eu^{3+}. The better energy level matching between high-energy Gd^{3+} and Eu^{3+} significantly enhances the energy transfer efficiency from $Gd^{3+} \rightarrow Eu^{3+}$. Therefore, in **Figure. 3b ii**, the characteristic emission of Gd^{3+} is nearly absent, and only the intense Eu^{3+} emission is observed. These processes work synergistically, achieving efficient energy transfer from $Gd^{3+} \rightarrow Eu^{3+}$ [39].

 doi:10.20944/preprints202502.0012.v1

Phosphor materials are often required to perform under diverse operational environments, with thermal stability being a critical factor, especially at elevated temperatures [40,41]. Higher temperatures intensify lattice vibrations, increase non-radiative relaxation pathways, and lead to reduced luminescence efficiency and fluorescence lifetime, culminating in thermal quenching [42]. However, the incorporation of substantial amounts of Gd^{3+} has been shown to effectively mitigate these issues. As demonstrated in **Figure 4a**, the temperature-dependent PL spectra of BYO: Eu^{3+} and BYGO: Eu^{3+} phosphors reveal that at 300 K, the emission intensity of BYO is 53.52% of BYGO. As the temperature increases to 450 K, this ratio decreases to 20.14%, indicating that BYO exhibits a faster decline in emission intensity. Within the practical operating temperature range for LEDs (~400 K), the emission intensity of BYGO retains 59.56% of its initial value at 300 K, whereas BYO retains only 20.26%, clearly highlighting the improved thermal stability conferred by Gd^{3+} doping. To investigate the underlying mechanism, the temperature-dependent fluorescence decay lifetimes of BYO: Eu^{3+} and BYGO: Eu^{3+} phosphors were measured, as shown in **Figure 4b**. The fluorescence lifetime (τ) was calculated using the method outlined in **Note S2**. As the temperature increases from 300 K to 450 K, under the detection conditions of an excitation wavelength of 258 nm and an emission wavelength of 612 nm, the τ of BYO: 5% Eu^{3+} decreases significantly from ~1.038 ms to ~0.774 ms. In contrast, under the same detection conditions, the τ of BYGO: 5% Eu^{3+}remains relatively stable at ~0.744 ms. In the undoped BYO: Eu^{3+} system, *2p* electrons of O^{2-} transfer energy to Eu^{3+} through the CTB, exciting its *4f* states [43]. The energy is subsequently dissipated via phonon-mediated non-radiative relaxation, a process that becomes increasingly pronounced at higher temperatures, leading to shorter excited-state lifetimes and diminished radiative efficiency. In contrast, the introduction of Gd^{3+} induces lattice expansion and increases structural asymmetry, effectively reducing lattice stress and defect density, thereby suppressing multi-phonon relaxation. Furthermore, the efficient energy transfer pathway from Gd^{3+} to Eu^{3+} enhances Eu^{3+} emission intensity while minimizing non-radiative relaxation [44]. This mechanism ensures that the BYGO system exhibits superior fluorescence lifetime stability at elevated temperatures, significantly mitigating thermal quenching effects.

The thermal activation energy (E_a), calculated using the Arrhenius equation, provides a quantitative measure of thermal quenching resistance. As shown in **Figure 4c**, the E_a of BYO: 5% Eu^{3+} is 0.1688 eV, while that of BYGO: 5% Eu^{3+} increases significantly to ~0.3051 eV. This value surpasses those reported for many red phosphors (see **Table S5**), underscoring the enhanced thermal stability of the BYGO system due to Gd^{3+} doping.

To further investigate the effect of Gd^{3+} doping on luminescent properties, **Figure 4d** illustrates the CIE chromaticity coordinates of BYO: 5% Eu^{3+} and BYGO: 5% Eu^{3+} at different temperatures. As the temperature increases, the CIE coordinates of BYO: 5% Eu^{3+} exhibit significant shifts, moving from the red region at (0.6382, 0.3258) to the orange region at (0.5951, 0.3008). This change is attributed to intensified lattice expansion at elevated temperatures, where the $^5D_0 \rightarrow {}^7F_2$ electric dipole transition at 612 nm, being more sensitive to the local coordination environment, undergoes faster thermal quenching compared to the $^5D_0 \rightarrow {}^7F_1$ magnetic dipole transition at ~538 nm. In contrast, BYGO: 5% Eu^{3+} maintains stable CIE coordinates at (0.6524, 0.3471) across the entire temperature range, benefiting from a more stable lattice structure and reduced influence of phonon energy on energy transfer. The CCT values, calculated using the method detailed in **Note S4** and summarized in **Table S6**, further corroborate this stability. The CCT of BYO: 5% Eu^{3+} varies between 3161 K and 3468 K, while BYGO: 5% Eu^{3+} consistently achieves a lower CCT of approximately 2700 K, which is favorable for improved color rendering [45]. These findings indicate that Gd^{3+} doping not only enhances luminescence intensity and efficiency but also significantly improves lattice stability and thermal resistance. Such advancements provide a novel design approach for lighting applications in dynamic and high-temperature environments.

 doi:10.20944/preprints202502.0012.v1

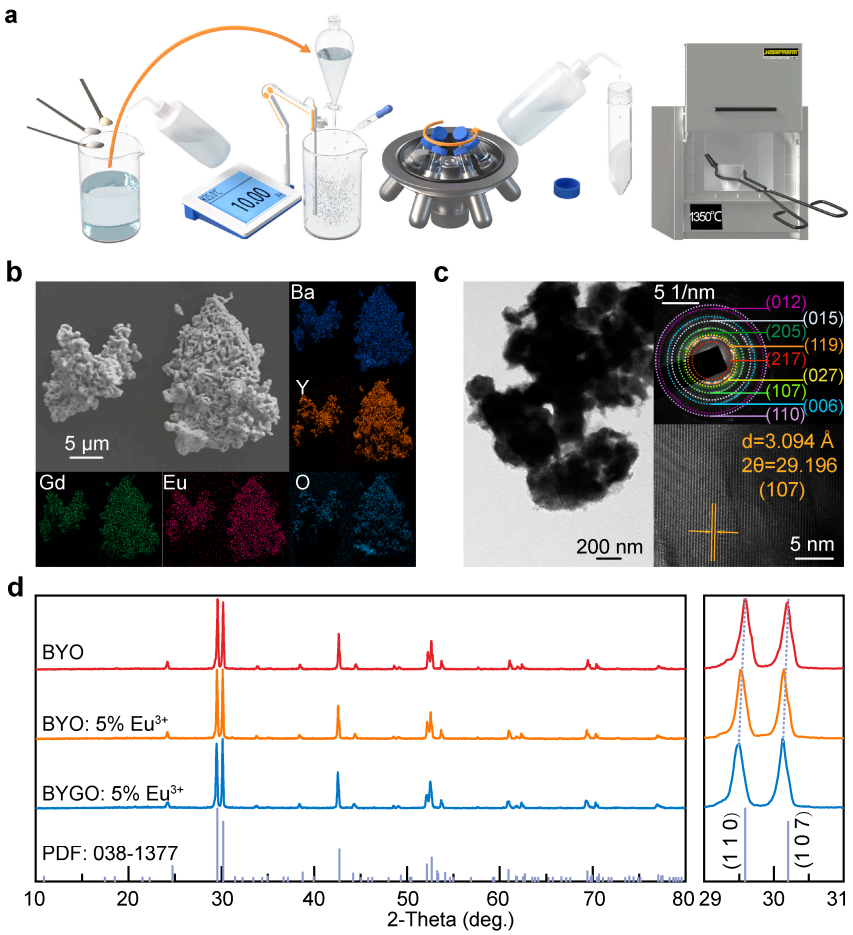

Figure 1. Synthesis and characterization of BYGO: Eu^{3+}.

Figure 1a Synthesis process of BYGO: Eu^{3+} phosphor. **Figure 1b** FE-SEM and EDS Mapping of BYGO: Eu^{3+} phosphor. **Figure 1c** FE-TEM analysis of BYGO: Eu^{3+} phosphor. **Figure 1d** XRD pattern of BYGO: Eu^{3+} phosphor, with an enlarged detail of the main peak on the right.

 doi:10.20944/preprints202502.0012.v1

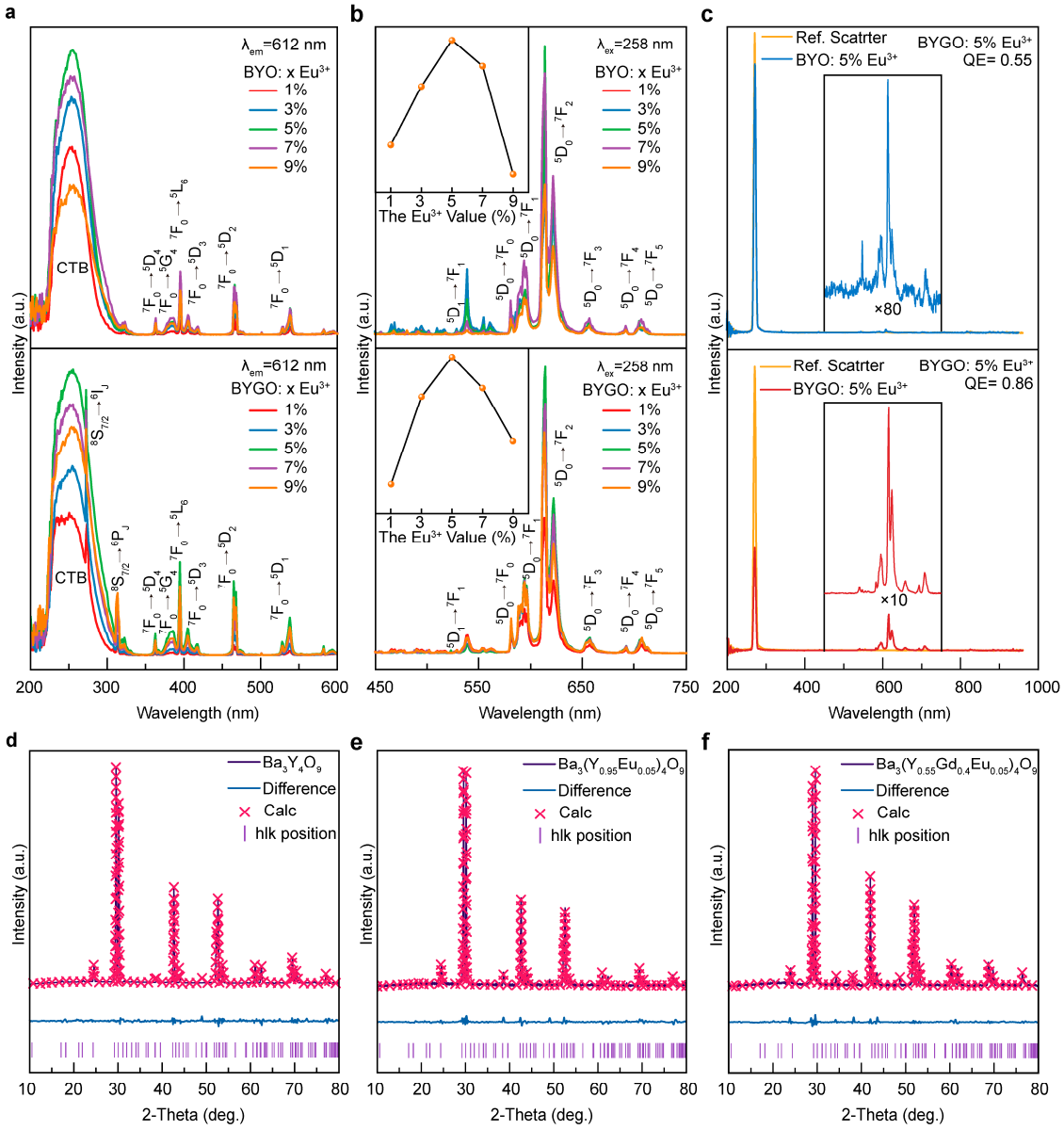

Figure 2. Optical characterization of BYGO: Eu^{3+} phosphor.

Figure 2a Comparison of the PLE spectra of BYO: Eu^{3+} and BYGO: Eu^{3+}. **Figure 2b** Comparison of the PL spectra of BYO: Eu^{3+} and BYGO: Eu^{3+}. **Figure 2c** Comparison of the quantum efficiency (QE) of BYO: 5% Eu^{3+} and BYGO: 5% Eu^{3+}. **Figure 2 d, e, f** XRD patterns of BYO, BYO: Eu^{3+}, and BYGO: Eu^{3+}, respectively, refined using the Topas software.

Preprints.org (www.preprints.org) | NOT PEER-REVIEWED | Posted: 3 February 2025 doi:10.20944/preprints202502.0012.v1

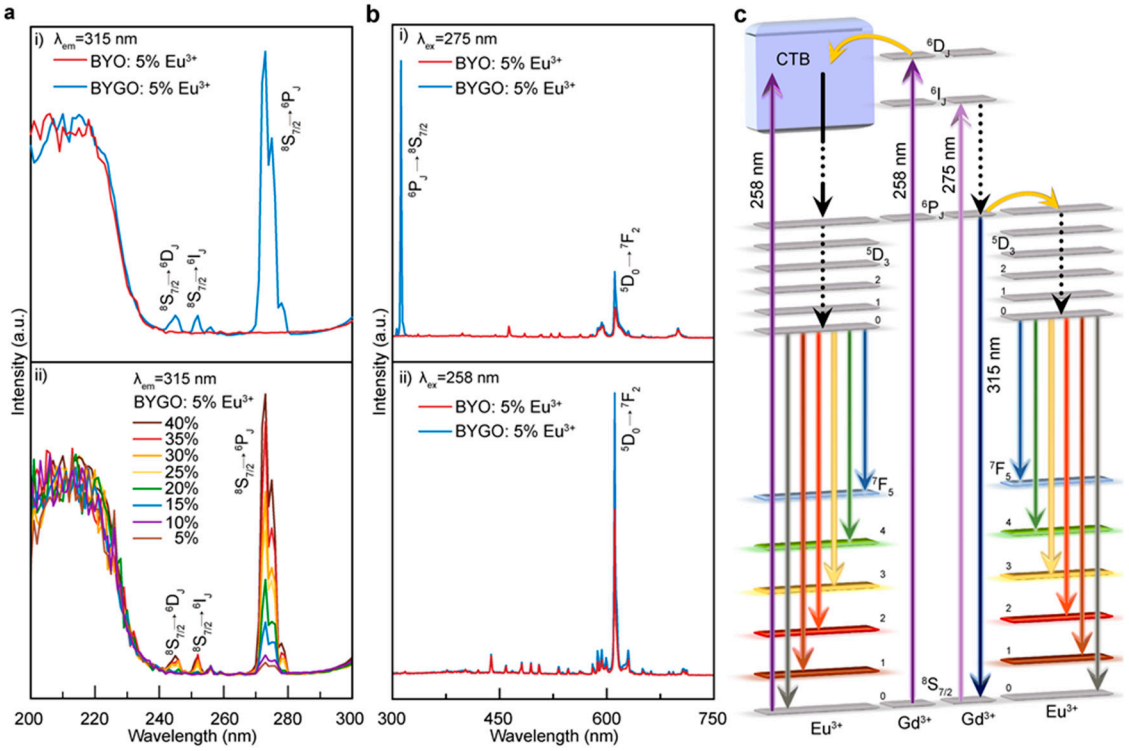

Figure 3. Energy transfer in BYGO: Eu^{3+} phosphor.

Figure 3a Comparison of PLE spectra with an excitation wavelength of 315 nm, i) comparison of the PLE spectra of BYO: 5% Eu^{3+} and BYGO: 5% Eu^{3+}, ii) comparison of PLE spectra with a fixed doping of 5% Eu^{3+} while varying the Gd content. **Figure 3b** comparison of the PL spectra of BYO: 5%Eu^{3+} and BYGO: 5% Eu^{3+} at different excitation wavelengths, i) comparison of PL spectra at a excitation wavelength of 275 nm, ii) comparison of PL spectra at the normal excitation wavelength of 258 nm. **Figure 3c** Schematic diagram of energy transfer in the BYGO: 5% Eu^{3+} system.

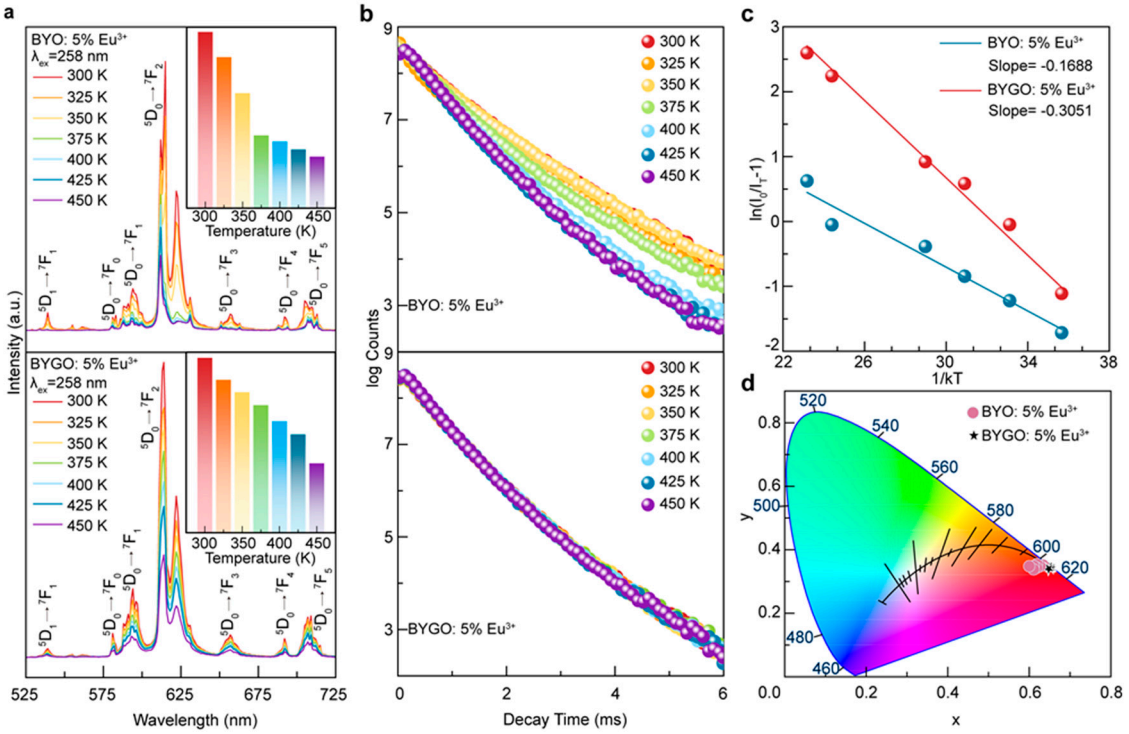

Figure 4. Comparison of luminescent properties of BYO: 5% Eu^{3+} and BYGO: 5% Eu^{3+} at different temperatures.

 doi:10.20944/preprints202502.0012.v1

Figure 4a Comparison of photoluminescence (PL) spectra of BYO: 5% Eu^{3+} and BYGO: 5% Eu^{3+} at different temperatures. **Figure 4b** Comparison of PL spectra of BYO: 5% Eu^{3+} and BYGO: 5% Eu^{3+} at different temperatures. **Figure 4c** Thermal quenching activation energy of BYO: 5% Eu^{3+} and BYGO: 5% Eu^{3+}. **Figure 4d** CIE color coordinates of BYO: 5% Eu^{3+} and BYGO: 5% Eu^{3+} at different temperatures.

3. Materials and Methods

Barium nitrate ($Ba(NO_3)_2$, 99.999%), yttrium nitrate hexahydrate ($Y(NO_3)_3{\cdot}6H_2O$, 99.99%), gadolinium nitrate hexahydrate ($Gd(NO_3)_3{\cdot}6H_2O$, 99.99%), and europium nitrate hexahydrate ($Eu(NO_3)_3{\cdot}6H_2O$, 99.99%) were procured from Alfa Aesar (China) Chemical Co., Ltd. Ammonium bicarbonate (NH_4HCO_3, 99.995%), n-hexane (C_6H_{14}, UV/VIS spectroscopy grade), and absolute ethanol (CH_3CH_2OH, 99.8%) were supplied by Shanghai Aladdin Biochemical Technology Co., Ltd. All reagents were of analytical grade and used as received without further purification.

For each synthesis of the BYGO: Eu^{3+} precursor, stoichiometric amounts of nitrate salts were precisely weighed according to their atomic ratios and dissolved in ultrapure water to prepare 250 mL of solution. This solution was slowly added dropwise into an ammonium bicarbonate solution while maintaining a constant pH of 10 by the controlled addition of dilute ammonium hydroxide. After the titration, the suspension was stirred continuously for 6 hours to ensure complete homogenization. The resulting precipitate was washed thoroughly with deionized water and n-hexane to remove impurities, followed by drying at 65 °C for 6 hours to obtain the precursor powder. The dried precursor was calcined in a muffle furnace (Nabertherm LHT 08-18, Germany) at a heating rate of 1 °C/min. The temperature was raised to 1350 °C and maintained for 5 hours. At the end of the calcination process, the phosphor samples were extracted from the furnace at 1350 °C and rapidly cooled to room temperature to facilitate phase transformation. The cooled phosphor powders were ground finely using an agate mortar and pestle and then sieved through a 1000-mesh stainless steel sieve (15 μm pore size) to achieve uniform particle size distribution.

The surface morphology of the phosphor materials was examined using a field emission scanning electron microscope (FE-SEM, Hitachi SU-70) equipped with an energy-dispersive spectroscopy (EDS) system operated at an accelerating voltage of 5 kV to analyze elemental composition. The nanoscale characteristics and lattice spacings of the samples were further analyzed by field emission transmission electron microscopy (FE-TEM, JEM-F200, JEOL). Selected area electron diffraction (SAED) patterns were also acquired using the TEM's integrated detector. X-ray diffraction (XRD) analysis of all samples was performed using a Rigaku SmartLab XRD system. Scans were conducted from 10° to 90° in 2θ, with a step size of 0.02° and a scanning speed of 0.05 seconds per step under ambient conditions (Cu Kα radiation, λ = 1.5412 Å). Structural refinement of the XRD data was carried out using the Le Bail method with Topas3 software to determine the crystal structure. Photoluminescence (PL) emission, photoluminescence excitation (PLE), and fluorescence decay curves were recorded using an Edinburgh Instruments FLS-1000 fluorimeter. Quantum efficiency (QE) was measured using a Horiba DeltaFlex instrument equipped with a 260 nm NanoLED laser, enabling precise evaluation of the phosphor's photoluminescent properties.

4. Conclusions

A series of BYO: Eu^{3+} phosphors were synthesized via co-precipitation, and doping with ~40% Gd^{3+} led to significant improvements in both luminescent performance and thermal stability. Structural analysis confirmed that Gd^{3+} substitution for Y^{3+} caused a lattice expansion of approximately 4.0%, which enhanced the energy transfer from Gd^{3+} to Eu^{3+}, resulting in increased Eu^{3+} emission intensity. The quantum efficiency of BYGO: 5% Eu^{3+} reached ~86%, notably higher than the ~55% observed for BYO: 5% Eu^{3+}. Thermal activation energy (E_a) for BYGO: Eu^{3+} was calculated to be ~0.3051 eV, significantly surpassing the ~0.1688 eV for BYO: Eu^{3+}, indicating improved resistance to thermal quenching. Even at elevated temperatures (300 K to 450 K), BYGO: Eu^{3+} maintained a stable

 doi:10.20944/preprints202502.0012.v1

fluorescence lifetime (~0.744 ms) and a consistent color temperature (~2066 K), reflecting enhanced high-temperature color stability. These findings demonstrate that Gd^{3+} doping substantially improves the thermal and optical properties of the BYGO: Eu^{3+} system, making it highly promising for high-temperature applications in LED lighting and display technologies.

Supplementary Materials: The following supporting information can be downloaded at: Preprints.org, Figure S1: title; Table S1: title; Video S1: title. **Figure S1** FE-SEM images of a single BYGO: 5% Eu^{3+} precursor (a) and the same precursor after calcination at 1350°C (b), showing significant morphological changes due to thermal treatment; **Figure S2** Comparison of emission intensity between Eu^{3+}-doped BYO and BYGO systems; **Figure S3** Comparison of QE between BYO: Eu^{3+} and BYGO: Eu^{3+}; **Figure S4** XRD of $Ba_3Y_2Gd_{1.8}Eu_{0.2}O_9$; **Table S1** Crystal structure data interpretation of $Ba_3Y_4O_9$, $Ba_3Y_{3.8}Eu_{0.2}O_9$ and $Ba_3Y_{2.2}Gd_{1.6}Eu_{0.2}O_9$ phosphor with reference to standard $Ba_3Y_4O_9$ host at room temperature 25 ^oC; **Table S2** Diverse atomic parameters together with the refined atomic positions of $Ba_3Y_4O_9$ phosphor; **Table S3** Diverse atomic parameters together with the refined atomic positions of $Ba_3Y_{3.8}Eu_{0.2}O_9$ phosphor; **Table S4** Diverse atomic parameters together with the refined atomic positions of $Ba_3Y_{2.2}Gd_{1.6}Eu_{0.2}O_9$ phosphor; **Table S5** Comparison of activation energy of the BYGO phosphor with some previously reported phosphors; **Table S6** Colour temperature statistics of the samples; **Note.S1** Quantum yields; **Note S2** Decay time; **Note S3** Activation Energy; **Note S4** Colour temperature.

Author Contributions: Conceptualization, Dong Zhu and Youming Lu; methodology, Chunfeng Wang; software, Shun Han; validation, Peijiang Cao, Dong Zhu and Yuxiang Zeng; formal analysis, Dong Zhu and Youming Lu; investigation, Peijiang Cao; resources, Chunfeng Wang and Deliang Zhu; data curation, Dong Zhu and Youming Lu; writing—original draft preparation, Dong Zhu and Youming Lu; writing—review and editing, Dong Zhu and Youming Lu; visualization, Zhu and Yuxiang Zeng; supervision, Wenjun Liu; project administration, Deliang Zhu; funding acquisition, Youming Lu All authors have read and agreed to the published version of the manuscript.

Funding: This work was supported by the National Natural Science Foundation of China (Grant No. 52372154, 12074263, 51872187, and U22A2077), the Natural Science Foundation of Guangdong Province (Grant No. 2021A1515012013), the Shenzhen Science and Technology Innovation Commission (Grant No. JCYJ20240813142628038, JCYJ20220809152330002, JCYJ20180305124701756, JCYJ20180508163404043, JCYJ20180305071822489 25), and the Shenzhen High-End Talent Scientific Research Program.

Informed Consent Statement: Informed consent was obtained from all subjects involved in the study.

Data Availability Statement: The original contributions presented in this study are included in the article/supplementary material. Further inquiries can be directed to the corresponding authors.

Conflicts of Interest: The authors declare no conflicts of interest.

Abbreviations

The following abbreviations are used in this manuscript:

W-LEDs	White light-emitting diodes
BYO	$Ba_3Y_4O_9$
BYGO	$Ba_3(Y_{0.6}Gd_{0.4})_4O_9$
CCT	Correlated color temperature
CTB	Charge transfer band
PL	Photoluminescence
PLE	photoluminescence excitation
QE	Quantum efficiency
FE-SEM	Field emission scanning electron microscope
EDS	energy-dispersive spectroscopy
FE-TEM	Field emission transmission electron microscopy
SAED	Selected area electron diffraction
XRD	X-ray diffraction
E_a	Activation energy

 doi:10.20944/preprints202502.0012.v1

References

1. Lin, S. S.; Lin, H.; Huang, Q. M.; Yang, H. Y.; Wang, B.; Wang, P. F.; Sui, P.; Xu, J.; Cheng, Y.; Wang, Y. S., Highly crystalline $Y_3Al_5O_{12}$: Ce^{3+} phosphor in glass film: A new composite color converter for next generation high brightness laser driven lightings. *Laser Photonics Rev.* 2022, *16*, 2200523.
2. Wu, H. Y.; Li, H. M.; Jiang, L. H.; Pang, R.; Zhang, S.; Li, D.; Liu, G. Y.; Li, C. Y.; Feng, J.; Zhang, H. J., Design of a mixed-anionic-ligand system for a blue-light-excited orange-yellow emission phosphor $Ba_{1.31}Sr_{3.69}(BO_3)_3Cl$: Eu^{2+}. *J. Mater. Chem. C,* 2020, *8*, 3040-3050.
3. Ryu, J. E.; Park, S.; Park, Y.; Ryu, S. W.; Hwang, K.; Jang, H. W., Technological breakthroughs in chip fabrication, transfer, and color conversion for high-performance micro-LED displays. *Adv. Mater.* 2023, *35*, 2204947.
4. Lee, J.; Min, K.; Park, Y.; Cho, K. S.; Jeon, H., Photonic crystal phosphors integrated on a blue LED chip for efficient white light generation. *Adv. Mater.* 2018, *30*, 1703506.
5. Bispo-Jr, A. G.; Saraiva, L. F.; Lima, S. A.; Pires, A. M.; Davolos, M. R., Recent prospects on phosphor-converted LEDs for lighting, displays, phototherapy, and indoor farming. *J. Lumin.* 2021, *237*, 118167.
6. Zhang, W.; Wang, C.; Qiao, X.; Fan, X., Simultaneous enhancement of red luminescence and thermal stability of a novel red phosphor: A Li^+-Eu^{3+} co-occupied site strategy in $BaAl_2Ge_2O_8$ lattices. *J. Rare Earth.*2024, *42*, 1846-1854.
7. Du, P.; Tang, J.; Li, W.; Luo, L.; Runowski, M., Manipulating concentration quenching and thermal stability of Eu3+-activated NaYbF4 nanoparticles via phase transition strategy toward diversified applications. Mater. Today Chem. 2022, 26, 101013.
8. Jahanbazi, F.; Mao, Y. B., Recent advances on metal oxide-based luminescence thermometry. *J. Mater. Chem. C*, 2021, *9*, 16410-16439.
9. Zhou, Z.; Zhu, H.; Huang, X.; She, Y.; Zhong, Y.; Wang, J.; Liu, M.; Li, W.; Xia, M., Anti-thermal-quenching, color-tunable and ultra-narrow-band cyan green-emitting phosphor for w-LEDs with enhanced color rendering. *Chem. Eng. J.* 2022, *433*, 134079.
10. Sun, L.; Liu, Y.; Wang, B.; Yang, S., Emerging near-unity internal quantum efficiency and color purity from red-emitting phosphors for warm white LED with enhanced color rendition. *J. Alloy. Compd.* 2022, *899*, 163209.
11. Ma, Y.; Li, Y.; Yu, H.; Lv, Z.; Guan, X.; Yu, J.; Ma, S.; Xia, L.; Dong, X., Design strategies of rare-earth luminescent complexes with zero thermal quenching protected by the wire-in-tube structure and the construction of a W-WLED with highly stable illumination and colour reproduction. *J. Mater. Chem. C,* 2024, *12*, 17278-17288.
12. Geng, X.; Xie, Y.; Chen, S.; Luo, J.; Li, S.; Wang, T.; Zhao, S.; Wang, H.; Deng, B.; Yu, R., Enhanced local symmetry achieved zero-thermal-quenching luminescence characteristic in the Ca_2InSbO_6: Sm^{3+} phosphors for w-LEDs. *Chem. Eng. J.* 2021, *410*, 128396.
13. Hooda, A.; Khatkar, A.; Boora, P.; Singh, S.; Devi, S.; Khatkar, S.; Taxak, V., Structural, optical and morphological features of combustion derived $Ba_3Y_4O_9$: Dy^{3+} nanocrystalline phosphor with white light emission. *Optik*, 2021, *228*, 166176.
14. Hooda, A.; Khatkar, S.; Khatkar, A.; Malik, R.; Kumar, M.; Devi, S.; Taxak, V., Reddish-orange light emission via combustion synthesized $Ba_3Y_4O_9$: Sm^{3+} nanocrystalline phosphor upon near ultraviolet excitation. *J. Lumin.* 2020, *217*, 116806.
15. Hooda, A.; Khatkar, S. P.; Devi, S.; Taxak, V. B., Structural and spectroscopic analysis of green glowing down-converted BYO: Er^{3+} nanophosphors for pc-WLEDs. *Ceram, Int*, 2021, *47*, 25602-25613.
16. Xing, G. C.; Gao, Z. Y.; Tao, M. X.; Wei, Y.; Liu, Y. X.; Dang, P. P.; Li, G. G.; Lin, J., Novel orange-yellow-green color-tunable Bi^{3+}-doped $Ba_3Y_{4-w}Lu_wO_9$ ($0 \le w \le 4$) luminescent materials: site migration and photoluminescence control. *Inorg. Chem. Front.* 2019, *6*, 3598-3603.
17. Han, X. Y.; Hu, C. Q.; Wu, J. M.; Wang, S. X.; Ye, Z. M.; Yang, Q. C., Systematical site investigation and temperature sensing in Pr^{3+}-doped $M_3Re_4O_9$ (M = Sr and Ba; RE = Sc, Y, Lu). *Chem. Eng. J.* 2023, *452*, 139159.
18. Liang, J.; Sun, L. L.; Annadurai, G.; Devakumar, B.; Wang, S. Y.; Sun, Q.; Qiao, J. L.; Guo, H.; Li, B.; Huang, X. Y., Synthesis and photoluminescence characteristics of high color purity $Ba_3Y_4O_9$: Eu^{3+} red-emitting phosphors with excellent thermal stability for warm W-LED application. *RSC Adv.* 2018, *8*, 32111-32118.

19. Li, K.; Lian, H. Z.; Shang, M. M.; Lin, J., A novel greenish yellow-orange red $Ba_3Y_4O_9$: Bi^{3+}, Eu^{3+} phosphor with efficient energy transfer for UV-LEDs. *Dalton T.* 2015, *44*, 20542-20550.
20. Zinchenko, V.; Volchak, G.; Chivireva, N.; Doga, P.; Bobitski, Y.; Ieriomin, O.; Smola, S.; Babenko, A.; Sznajder, M., Solidified salt melts of the NaCl-KCl-CeF_3-EuF_3 system as promising luminescent materials. *Materials,* 2024, *17*, (22).
21. Nikiforov, I. V.; Spassky, D. A.; Krutyak, N. R.; Shendrik, R. Y.; Zhukovskaya, E. S.; Aksenov, S. M.; Deyneko, D. V., Co-doping effect of Mn^{2+} and Eu^{3+} on luminescence in strontiowhitlockite phosphors. *Molecules,* 2024, *29*, 124.
22. Mortensen, S. S.; Nielsen, V. R. M.; Sorensen, T. J., Contrasting impact of coordination polyhedra and site symmetry on the electronic energy levels in nine-coordinated Eu^{3+} and Sm^{3+} crystals structures determined from single crystal luminescence spectra. *Dalton T.* 2024, *53*, 10079-10092.
23. Ichiba, K.; Kato, T.; Watanabe, K.; Takebuchi, Y.; Nakauchi, D.; Kawaguchi, N.; Yanagida, T., Evaluation of photoluminescence and scintillation properties of Eu-doped YVO_4 single crystals synthesized by optical floating zone method. *J. Lumin.* 2024, *266*, 120327.
24. Chen, Y. Q.; Guo, H. J.; Shi, Q. F.; Qiao, J. W.; Cui, C. E.; Huang, P.; Wang, L., Single-band ratiometric thermometry strategy based on the completely reversed thermal excitation of $O^{2-} \rightarrow Eu^{3+}$ CTB edge and Eu^{3+} *4f* → *4f* transition. *Inorg. Chem.* 2024, *63*, 16304-16312.
25. Huang, C. H.; Chen, C. T.; Guo, S. Q.; Zhang, J. Y.; Liu, W. R., Luminescence and theoretical calculations of novel red-emitting $NaYPO_4F$: Eu^{3+} phosphor for LED applications. *J. Alloy. Compd.* 2017, *712*, 225-232.
26. Xiang, L.; Zhou, X. J.; Li, L.; Ling, F. L.; Li, Y. H.; Li, J. F.; Yang, H. M., Comparative study on the anomalous intense $^5D_0 \rightarrow {}^7F_4$ emission in Eu^{3+} doped Sr_2MNbO_6 (M=Ga, In, Gd) phosphors. *J. Lumin.* 2024, *267*, 120370.
27. Li, H.; Niu, Y. F.; Liu, C. L.; Jiang, H. M.; Li, J. P.; Wu, J. Z.; Huang, S. P.; Zhang, H. Z.; Zhu, J., Unraveling the Remarkable Influence of Square Antiprism Geometry on Highly Efficient Far-Red Emission of Eu³⁺ in Borotellurate Phosphors for Versatile Utilizations. *Laser Photonics Rev.* 2024, *12*, 2400843.
28. Mancic, L.; Lojpur, V.; Marinkovic, B. A.; Dramicanin, M. D.; Milosevic, O., Hydrothermal synthesis of nanostructured Y_2O_3 and $(Y_{0.7}Gd_{0.25})_2O_3$ based phosphors. *OPTICAL MATERIALS* **2013,** 35, (10), 1817-1823.
29. Liu, G. Y.; Liu, B.; Li, J. K.; Liu, Z. M., Synthesis and luminescent properties of $Ba_3Y_{3.88}Gd_{0.12}O_9$: Eu^{3+} phosphors with enhanced red emission. *J. Rare Earth. 2022*, 40, 534-540.
30. Qin, K. L.; Sun, J. B.; Zhu, X. D.; Cao, F. B.; Liu, W. M.; Shen, X. M.; Wu, X. R.; Wu, Z. J., Eu^{3+} doped high-aluminum cast residue prepared $EuCaAl_3O_7/Ca_2Al_2SiO_7$ luminescent material with $^5D_0 \rightarrow {}^7F_2/{}^5D_0 \rightarrow {}^7F_4$ double red intense emission. *J. Lumin.* 2021, *233*, 117920.
31. Wu, C. C.; Chen, K. B.; Lee, C. S.; Chen, T. M.; Cheng, B. M., Synthesis and VUV photoluminescence characterization of $(Y,Gd)(V,P)O_4$: Eu^{3+} as a potential red-emitting PDP phosphor. CHEMISTRY OF MATERIALS 2007, *19*, 3278-3285.
32. Khan, N. Z.; Khan, S. A.; Muhammad, N.; Chen, W. L.; Ahmed, J.; Padhiar, M. A.; Chen, M.; Runowski, M.; Alshehri, S. M.; Zhang, B. H.; Pan, S. S.; Zheng, R. K., Tunable single-phase white light emission from complex perovskite $Sr_3CaNb_2O_9$: Dy^{3+}/Eu^{3+} phosphors. *Adv. Opt. Mater.* 2025, *13*, 2401938.
33. Pawlik, N.; Szpikowska-Sroka, B.; Goryczka, T.; Pisarski, W. A., Studies of energy transfer process between Gd^{3+} and Eu^{3+} ions in oxyfluoride sol-gel materials. *Ceram. Int.* 2023, *49*, 41041-41053.
34. Verma, N.; Michalska-Domanska, M.; Dubey, V.; Ram, T.; Kaur, J.; Dubey, N.; Aman, S.; Manners, O.; Saji, J., Investigation of spectroscopic parameters and trap parameters of Eu^{3+}-activated Y_2SiO_5 phosphors for display and dosimetry applications. Molecules 2025, *30*, 108.
35. Hu, A.; Jiang, Y.; An, J.; Huang, X.; Elgarhy, A. H.; Cao, H.; Liu, G., Novel Fe/Ca oxide co-embedded coconut shell biochar for phosphorus recovery from agricultural return flows. *RSC Adv.* 2024, *14*, 27204-27214.
36. Martins, F. C. B.; Firmino, E.; Oliveira, L. S.; Dantas, N. O.; Silva, A. C. A.; Barbosa, H. P.; Rezende, T. K. L.; Góes, M. S.; dos Santos, M. A. C.; de Oliveira, L. F. C.; Ferrari, J. L., Development of Y_2O_3:Eu^{3+} materials doped with variable Gd^{3+} content and characterization of their photoluminescence properties under UV excitation. *Mater. Chem. Phys.* **2022,** *277*, 125498.

 doi:10.20944/preprints202502.0012.v1

37. Liu, Q.; Li, X. B.; Guo, J. K.; Wang, L. X.; Song, J. K.; Zhang, Q. T., Second-order John-Teller distortion in the thermally stable Li(La, Gd) $MgWO_6$:Eu^{3+} phosphor with high quantum efficiency. *Dyes Pigments* **2019,** *160*, 165-171..
38. Bhagyalekshmi, G. L.; Ganesanpotti, S., Comprehension of the photoinduced charge transfer assisted energy transfer in Gd^{3+}-based host sensitized tellurate phosphors for thermal sensing and anticounterfeiting labels. *Dalton T.* 2024, *53*, 8229-8242.
39. Bazzi, R.; Flores, M. A.; Louis, C.; Lebbou, K.; Zhang, W.; Dujardin, C.; Roux, S.; Mercier, B.; Ledoux, G.; Bernstein, E.; Perriat, P.; Tillement, O., Synthesis and properties of europium-based phosphors on the manometer scale: Eu_2O_3, Gd_2O_3: Eu, and Y_2O_3: Eu. *J. Colloid Interface Sci.* 2004, *273*, 191-197.
40. Brites, C. D. S.; Balabhadra, S.; Carlos, L. D., Lanthanide-based thermometers: At the cutting-edge of luminescence thermometry. *Adv. Opt. Mater.* 2019, *7*, 1801239.
41. Qiao, J. W.; Zhang, S.; Zhou, X. Q.; Chen, W. B.; Gautier, R.; Xia, Z. G., Near-infrared light-emitting diodes utilizing a europium-activated calcium oxide phosphor with external quantum efficiency of up to 54.7%. *Adv. Mater.* 2022, *34*, 2201887.
42. Zhuo, Y.; Tehrani, A. M.; Oliynyk, A. O.; Duke, A. C.; Brgoch, J., Identifying an efficient, thermally robust inorganic phosphor host via machine learning. *Nat. Commun.* 2018, *9*, 4377.
43. Ye, W. G.; Zhao, C.; Shen, X. F.; Ma, C. Y.; Deng, Z. H.; Li, Y. B.; Wang, Y. Z.; Zuo, C. D.; Wen, Z. C.; Li, Y. K.; Yuan, X. Y.; Wang, C.; Cao, Y. G., High quantum yield $Gd_{4.67}Si_3O_{13}$: Eu^{3+} red-emitting phosphor for tunable white light-emitting devices driven by UV or blue LED. *ACS Appl. Electron. Mater.* 2021, *3*, 1403-1412.
44. Huang, X.; Zhang, W. T.; Wang, X. M.; Zhang, J. Y.; Gao, X.; Du, H. Y., Structure and luminescence investigation of Gd^{3+}-sensitized perovskite $CaLa_4Ti_4O_{15}$: Eu^{3+}: A novel red-emitting phosphor for high-performance white light-emitting diodes and plants lighting. *J. Colloid Interface Sci.* 2022, *608*, 3204-3217.
45. Dang, P. P.; Li, G. G.; Yun, X. H.; Zhang, Q. Q.; Liu, D. J.; Lian, H. Z.; Shang, M. M.; Lin, J., Thermally stable and highly efficient red-emitting Eu^{3+}-doped $Cs_3GdGe_3O_9$ phosphors for WLEDs: non-concentration quenching and negative thermal expansion. *Light-science & Applications*, 2021, 10, 29.